Mathematical Biosciences 360 (2023) 109012

Contents lists available at ScienceDirect

Mathematical Biosciences

journal homepage: www.elsevier.com/locate/mbs

Original Research Article

Coupling dynamics of 2D Notch-Delta signalling

Francisco Berkemeier [a,*], Karen M. Page [b]

[a] Department of Pathology, University of Cambridge, UK
[b] Department of Mathematics and IPLS, University College London, UK

ARTICLE INFO

Keywords:
Notch
Signalling
Stability
Protrusions
Lateral inhibition

ABSTRACT

Understanding pattern formation driven by cell–cell interactions has been a significant theme in cellular biology for many years. In particular, due to their implications within many biological contexts, lateral-inhibition mechanisms present in the Notch-Delta signalling pathway led to an extensive discussion between biologists and mathematicians. Deterministic and stochastic models have been developed as a consequence of this discussion, some of which address long-range signalling by considering cell protrusions reaching non-neighbouring cells. The dynamics of such signalling systems reveal intricate properties of the coupling terms involved in these models. In this work, we investigate the advantages and drawbacks of a single-parameter long-range signalling model across diverse scenarios. By employing linear and multi-scale analyses, we discover that pattern selection is not only partially explained but also depends on nonlinear effects that extend beyond the scope of these analytical techniques.

1. Introduction

In epithelial tissue, depending on the nature of the contact between cells, the Notch-Delta signalling pathway leads to fundamentally different patterns [1–3]. In highly packed epithelial layers, some cells have the ability to create extensions of themselves, developing protrusions that reach non-neighbouring cells and yielding a new and fundamental factor in the signalling dynamics. These basal actin-based filopodia are elongated and oriented in different directions, extending signalling to second or third neighbour cells [4–8].

In recent years, long-range signalling via filopodia has been shown to significantly impact the distribution and sparse patterning of sensory organ precursor (SOP) cells in the fly notum [9–11]. In other work, spatiotemporal patterns of spinal neuron differentiation were revealed to be mediated by basal protrusions [12]. In contrast to the frequently observed short-ranged patterns induced by short-range signalling, cell protrusions result in sparser SOP cell patterning.

The stochastic nature of these biological systems crucially affects patterning. For example, noise arising from dynamic protrusions has been shown to have a significant role in pattern refinement when studying the organisation of bristles on the *Drosophila melanogaster* notum [9]. A cellular automaton model of cell–cell signalling revealed that rule-dependent structured noise also triggers refined and biased patterning [10], hinting at the self-organising nature of such systems. Intrinsic noise, driven by stochastic gene expression, has been studied via the Chemical Langevin Equation [13] and shown to directly affect juxtacrine-based pattern formation [14].

In addition to constructing realistic long-range signalling models capable of numerically describing long-range patterning, linear stability analysis (LSA) has revealed inherent characteristics of lateral inhibition models [15–17]. Biased and long-range signalling was also studied in [18], where weight-based coupling functions were considered for several one-dimensional signalling systems. We aim to partially extend this work by studying the two-dimensional hexagonal array under specific signalling weights.

In 1996, Joanne Collier and colleagues developed the first model of Notch-mediated lateral inhibition [19]. In this work, the authors considered purely juxtacrine signalling dynamics, where the signalling cell and the target cell are in direct physical contact. We define a model of long-range Notch-Delta signalling, which is a relative weight-based extension of the original Collier model, and name it the ϵ-Collier model. We introduce a weighting parameter ϵ that relatively weights juxtacrine and long-range signalling contributions, creating a complex non-local signalling network.

Under different filopodium behaviour and lifespan assumptions, one can explore the robustness of the extended Collier model via LSA, providing a general framework for analysing autonomous systems of signalling cells, as detailed in Supplementary Note 1 (SN1). Furthermore, such a parameterised model allows us to investigate the limits on cell coupling sufficient to obtain long-range patterns. In parallel, we explore the effects of stochastic filopodium dynamics on patterning. Finally, we expand some of the techniques from LSA to describe a general framework for multiple-scale methods and weakly nonlinear

* Correspondence to: Department of Pathology, University of Cambridge, 10 Tennis Court Road, Cambridge, CB2 1QP, UK.
E-mail address: fp409@cam.ac.uk (F. Berkemeier).

https://doi.org/10.1016/j.mbs.2023.109012

Available online 2 May 2023

stability analysis (WNSA) of coupled and decoupled dynamical systems (SN2).

In this paper, we first present the Collier model of Notch-Delta signalling, followed by its extension to long-range signalling, which we call the ϵ-Collier model. We then perform a linear stability analysis of this system. The results of the LSA are compared with numerical simulations. The cases of longer/oriented protrusions and stochastic protrusions are analysed. In the latter case, we assume that protrusions link and unlink at random. Stochastic protrusions can lead to pattern refinement over time. We perform a numerical bifurcation analysis of the ϵ-Collier model, showing which modes are expected to grow near a bifurcation, and show that these accurately predict the results of numerical simulations there. Finally, we present a multiscale method for analysing weakly nonlinear dynamics, and show that it is difficult to apply to this system.

2. Main methods

2.1. Lateral inhibition

We consider a periodic $N \times M$ hexagonal lattice (hexagonal torus), where each cell has 6 neighbouring cells (see Fig. 1(a)). For a given cell, we assume juxtacrine signalling occurs with all 6 of its neighbours via the usual Collier model [19]. Here, the authors used experimental data to build an ordinary differential equation (ODE) model of the feedback loop between two adjacent cells induced by Notch signalling (lateral inhibition). The model consists of a system of coupled ODEs per cell. Denoting by n_i and d_i the levels of Notch and Delta activity in cell i, we have the following system

$$\frac{d}{dt}n_i = f(\langle d_i \rangle) - n_i \tag{1}$$

$$\frac{d}{dt}d_i = \nu(g(n_i) - d_i), \tag{2}$$

where $f, g : [0,\infty) \to [0,\infty)$ are continuous increasing and decreasing functions, respectively, often taken to be Hill functions

$$f(x) = \frac{x^k}{a + x^k} \tag{3}$$

$$g(x) = \frac{1}{1 + bx^h} \tag{4}$$

for $x \geq 0$ and $h, k \geq 1$. $r_t \equiv 1/a$ and b are the trans-interactions strength and ligand inhibition strength parameters, respectively[1]. $\nu > 0$ is the ratio between Notch and Delta decay rates, determining the strength of decay. Finally, $\langle d_i \rangle$ is the average level of Delta activity in the cells adjacent to cell i, that is,

$$\langle d_i \rangle = \frac{1}{|\mathbf{nn}(i)|} \sum_{j \in \mathbf{nn}(i)} d_j, \tag{5}$$

where the sum is taken over the nearest neighbours $\mathbf{nn}(i)$ of cell i and $|\mathbf{nn}(i)|$ is the total number of neighbours. In general, depending on the hexagonal lattice orientation, either N or M must be even to ensure periodicity. From the previous equations, one can see that the rate of production of Notch activity is an increasing function of the level of Delta activity in neighbouring cells. In contrast, the rate of production of Delta activity is a decreasing function of the level of activated Notch within the same cell. The production of Notch and Delta activity is balanced by decay.

[1] The quantity $a^{1/k}$ is the neighbour Delta activity level necessary for half-maximal Notch activation, while $b^{-1/h}$ is the Notch activity level necessary for half-maximal Delta inhibition.

2.2. Long-range signalling

In addition to lateral cell–cell signalling, we also consider the possibility of long-range signalling with respect to non-neighbouring cells. We loosely refer to cell protrusions as the main mechanism for general, isotropic long-range signalling, interchangeably using these terms. A detailed discussion of protrusion dynamics is presented in [20]. For now, our notion of protrusions remains relatively abstract. There are several ways to implement protrusion-cell signalling. As a first simplification, we assume $\langle d_i \rangle$ is the only term affected by long-range signalling and extend its definition to include non-neighbouring cells that contact cell i. We also investigate the cases where ligand density decays with distance and protrusions are stochastic.

In general, we consider the approach suggested in [18]. Here, the authors used a weighting function $\omega(s,r)$ defining the signalling level from a signaller cell s to a receiver cell r. ω determines which cells are connected through protrusions, defining a connectivity matrix whose entries yield the signalling intensity. In a simplistic protrusion model, all non-zero entries of such a matrix are equal. The weighting function ω captures the matrix information, and we may rewrite the interaction term as follows

$$\langle d_i \rangle = \sum_{j \in \mathbf{n}(i)} \omega(i,j) d_j, \tag{6}$$

where the sum is made over the neighbours of i, $\mathbf{nn}(i)$, and the non-neighbouring cells that are reached by the protrusions, $\mathbf{np}(i)$, of cell i. Such an array of indexes is defined as $\mathbf{n}(i) = \mathbf{nn}(i) \cup \mathbf{np}(i)$. The further assumption that each cell has a finite amount of active ligand to distribute at any given time point results in the following restriction

$$\sum_{j \in \mathbf{n}(i)} \omega(i,j) = \overline{\omega} < +\infty. \tag{7}$$

Although there is some freedom in the interpretation of $\overline{\omega}$, we assume $\overline{\omega} = 1$ for simplicity.

2.3. The ϵ-Collier model

Our model, hereafter named the ϵ-Collier model, extends the mathematical systems in [19] by considering the inclusion of long-range signalling via protrusions balanced by the relative weighting factor $\epsilon \in [0,1]$. We begin by weighting each signalling contribution, juxtacrine (ω_J) and protrusion-based (ω_P), by the factor ϵ, to define the combined weighting function

$$\omega \equiv (1-\epsilon)\omega_J + \epsilon\omega_P. \tag{8}$$

Eq. (6)–Eq. (8) define the ϵ-Collier model, considering protrusions of relative signalling intensity ϵ. Naturally, Eq. (8) is only interesting when ω_J and ω_P are restricted to $\mathbf{nn}(i)$ and $\mathbf{np}(i)$, respectively. For example, the case $\epsilon = 0$ and $\omega_J(i,j) = \chi_{\mathbf{nn}(i)}(j)/6$, where $\chi_{\mathbf{nn}(i)}$ is the indicator (or characteristic) function of the set $\mathbf{nn}(i)$, corresponds to the original Collier model.

2.4. Coupling dynamics

We perform a linear stability analysis to understand the criteria for pattern formation driven by Notch-Delta signalling. This is a useful tool to not only identify the regions of the parameter space for which spontaneous patterning of SOP cells occurs but also to determine the typical spacing between Delta-expressing cells, often called the characteristic length of the pattern or pattern wavelength [15,17,19]. Our analysis closely follows the methods outlined in [18,19,21] and Murray [22], for the two-dimensional hexagonal array, and is based on the framework presented in SN1.

Eq. (1)–Eq. (2) possesses a single positive homogeneous steady state (n^*, d^*). At this state, we have $f(g(n^*)) = n^*$ and $g(n^*) = d^*$, which is unique because $f(g(n))$ is monotonically decreasing for all $n \geq 0$. Then,

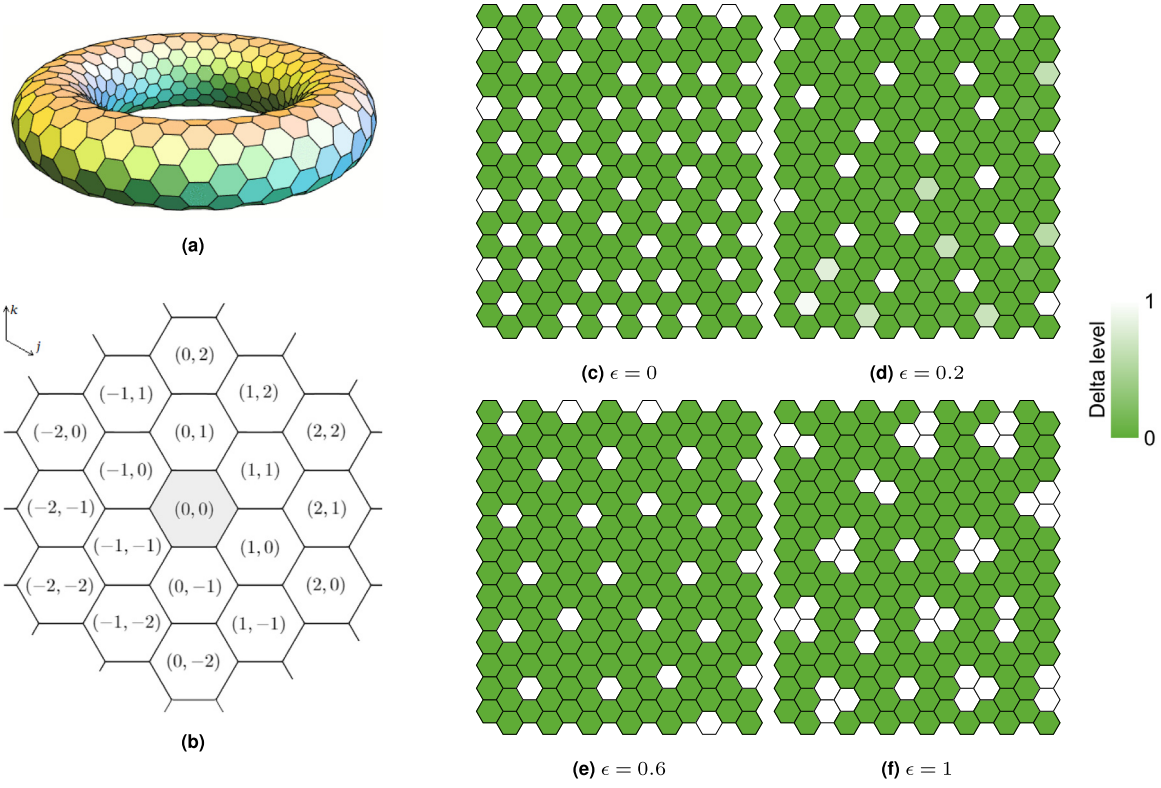

Fig. 1. Long-range Notch-Delta signalling on hexagonal lattices.
(a) Hexagonal torus. Periodic hexagonal lattices can be seen as hexagonal tori. **(b)** Hexagonal lattice main directions (j, k axes) and cell position indexation relative to a focal cell $(0, 0)$. Different cell labelling schemes yield equivalent formulations of $\Omega_{\bar{q},\bar{p}}$, as defined in Eq. (17). **(c–f)** Notch-Delta patterns on a 14×14 periodic lattice for varying ϵ. SOP cells (white, high Delta, low Notch) contrast with non-SOP cells (green, low Delta, high Notch). Here, $h = k = 6$, $a = 10^{-8}$, $b = 10^2$, and $\nu = 1$. Initial conditions $n_i(0)$ and $d_i(0)$ have arbitrary values close to the homogeneous steady state $(n^*, d^*) \simeq (0.744, 0.055)$.

for small perturbations $\tilde{n}_i = n_i - n^*$ and $\tilde{d}_i = d_i - d^*$, linearisation leads to

$$\frac{d}{dt}\tilde{n}_i = A\langle\tilde{d}_i\rangle - \tilde{n}_i \tag{9}$$

$$\frac{d}{dt}\tilde{d}_i = \nu B\tilde{n}_i - \nu\tilde{d}_i, \tag{10}$$

where $A = f'(g(n^*))$ is the signal trans-activation by the ligand and $B = g'(n^*)$ is the ligand inhibition by the signal. For a $N \times M$ periodic hexagonal lattice, with $1 \le j \le N$ and $1 \le k \le M$, the perturbations can be written as a discrete Fourier series

$$\tilde{n}_i \equiv \tilde{n}_{j,k} = \sum_{q=1}^{N}\sum_{p=1}^{M} \xi_{q,p} e^{2\pi \mathrm{i}(qj/N + pk/M)} \tag{11}$$

$$\tilde{d}_i \equiv \tilde{d}_{j,k} = \sum_{q=1}^{N}\sum_{p=1}^{M} \eta_{q,p} e^{2\pi \mathrm{i}(qj/N + pk/M)}, \tag{12}$$

where two subindexes have been used to refer to the spatial position of cell i within the two-dimensional hexagonal lattice (see Fig. 1(b)). For $1 \le q \le N$ and $1 \le p \le M$, the inverted transform is

$$\xi_{q,p} = \frac{1}{MN}\sum_{k=1}^{M}\sum_{j=1}^{N} \tilde{n}_{j,k} e^{-2\pi \mathrm{i}(qj/N + pk/M)} \tag{13}$$

$$\eta_{q,p} = \frac{1}{MN}\sum_{k=1}^{M}\sum_{j=1}^{N} \tilde{d}_{j,k} e^{-2\pi \mathrm{i}(qj/N + pk/M)}. \tag{14}$$

Finally, applying this change of variables to Eq. (9)–Eq. (10) leads to the following linear system of coupled ordinary differential equations

$$\frac{d}{dt}\begin{pmatrix}\xi_{q,p}\\ \eta_{q,p}\end{pmatrix} = L\begin{pmatrix}\xi_{q,p}\\ \eta_{q,p}\end{pmatrix}, \tag{15}$$

where matrix L is a specification of matrix $\mathbf{L}_{\bar{q},\bar{p}}$ in Eq. (S43), defined as

$$L = \begin{pmatrix} -1 & A\Omega_{\bar{q},\bar{p}} \\ \nu B & -\nu \end{pmatrix} \tag{16}$$

and $\Omega_{\bar{q},\bar{p}}$ is the function that takes into account the spatial coupling terms of Eq. (9)–Eq. (10) within the hexagonal lattice (in this case, $\Omega_{\bar{q},\bar{p}} \propto \left[\boldsymbol{\Omega}_{\bar{q},\bar{p}}\right]_{12}$, defined by Eq. (S42)). We have then turned Eq. (1)–Eq. (2) into a system of constant-coefficient linear differential equations described by Eq. (15), which has a straightforward family of solutions. For now, however, we focus on the coupling function $\Omega_{\bar{q},\bar{p}}$, which holds the main mechanisms behind the dynamics of juxtacrine and long-range signalling in our system.

$\Omega_{\bar{q},\bar{p}}$ varies according to the weighting function ω. Here, $\bar{q} = q/N$ and $\bar{p} = p/M$ define the discrete wavenumbers (Fourier modes) and thus solutions for $0 < \bar{q}, \bar{p} \le 1$ correspond to patterned solutions with corresponding pattern wavelengths $(1/\bar{q}, 1/\bar{p})$. We assume that connections between cells depend only on their relative positions in the lattice (Fig. 1(b)) and therefore, for a sender cell s in position (j, k) and a receiver cell r in position (j', k'), we set $\omega(s_{j,k}, r_{j',k'}) \equiv \omega(j'-j, k'-k) = \omega(\Delta j, \Delta k)$. Hence, $\Omega_{\bar{q},\bar{p}}$ is, in general, given by

$$\Omega_{\bar{q},\bar{p}} = \sum_{\Delta jk \in S} \omega(\Delta j, \Delta k) e^{2\pi \mathrm{i}(\bar{q}\Delta j + \bar{p}\Delta k)}, \tag{17}$$

where $\Delta jk = (\Delta j, \Delta k)$. Now, if we assume connections are symmetric, i.e, $\omega(\Delta j, \Delta k) = \omega(-\Delta j, -\Delta k)$, we have, by Example 1.1 in SN1,

$$\Omega_{\bar{q},\bar{p}} = \sum_{\Delta jk \in S} \omega(\Delta j, \Delta k)\cos(2\pi(\bar{q}\Delta j + \bar{p}\Delta k)). \tag{18}$$

The diagonalisation of L leads to the temporal eigenvalues

$$\lambda^{\pm}_{\bar{q},\bar{p}} = \frac{1}{2}\left[-(1+\nu) \pm \sqrt{(1+\nu)^2 - 4\nu(1 - AB\Omega_{\bar{q},\bar{p}})}\right]. \tag{19}$$

Then, since $\nu > 0$, $\lambda^{+}_{\bar{q},\bar{p}}$ is a positive real number if and only if $AB\Omega_{\bar{q},\bar{p}} > 1$. A and B are the slopes of the feedback functions f and g at the homogeneous steady state and $|AB|$ is defined as the feedback strength. If $|AB| = 0$, then the homogeneous solution is linearly stable, $\mathrm{Re}(\lambda^{\pm}_{\bar{q},\bar{p}}) < 0$, and thus no periodic pattern is expected to emerge. On the other hand, the feedback strength has to be sufficiently high for patterns to arise, that is, $|AB| > |1/\Omega_{\min}|$, where $\Omega_{\min}$ denotes the minimum of the real function $\Omega_{\bar{q},\bar{p}}$, so that $\mathrm{Re}(\lambda^{+}_{\bar{q},\bar{p}})$ is maximal. With $A > 0$, $B < 0$ and assuming $\Omega_{\min} < 0$, we expect patterned solutions provided

$$AB < \frac{1}{\Omega_{\min}}. \tag{20}$$

In particular, this feedback is controlled by the tuple (a, b, h, k) as follows

$$A = f'(g(n^*)) = \frac{akd^{*k-1}}{(a + d^{*k})^2} \tag{21}$$

$$B = g'(n^*) = -\frac{bhn^{*h-1}}{(1 + bn^{*h})^2}, \tag{22}$$

where, again, (n^*, d^*) is the homogeneous steady state, $r_t = 1/a$ is the trans-interactions strength and b is the ligand inhibition strength. (n^*, d^*) can be found by setting $\langle d_i \rangle = d_i$ and finding the intersection of the nullclines $n_i = f(d_i)$ and $d_i = g(n_i)$. Assuming for convenience $h = k$, this can be rewritten as

$$n^* = f(g(n^*)) \tag{23}$$

$$d^* = g(n^*), \tag{24}$$

which can be numerically solved for each triple (h, r_t, b) in the parameter space. Such a solution, together with Eq. (20), defines the discrete analogues of Turing spaces consisting of $r_t - b = h$ parameter regions where spontaneous patterns occur. Outside such regions, pattern formation is not expected, since all of the linear modes have negative growth rates.

We now explore different weighting functions to capture the effects of juxtacrine signalling and protrusions, and discuss what features of ω affect $\Omega_{\min}$. We recall that ω determines the family of systems Eq. (1)–Eq. (2) via the weighting dynamics defined by Eq. (6)–Eq. (8).

For a given cell on a hexagonal lattice, we denote the closest ring of order $k \in \mathbb{N}_0$ by R_k, such that R_0 the cell itself, R_1 are its 6 neighbouring cells, R_2 is the ring of 12 second-neighbour cells, and so forth. Notice that $|R_k| = 6k$ $(k > 0)$. We further expand the definition of S in SN1 by defining S_k as the relative index set of cells in R_k (according to Fig. 1(b)), that is,

$$\begin{cases} S_0 = \{(0,0)\} \\ S_1 = \{(\pm 1, 0), (0, \pm 1), \pm(1,1)\} \\ S_2 = \{(0, \pm 2), (\pm 2, 0), \pm(1,-1), \\ \qquad \pm(1,2), \pm(2,1), \pm(2,2)\} \\ \quad \vdots \end{cases}. \tag{25}$$

This notation will be used throughout this work. Notice that such a definition can be ambiguous in different contexts, as discussed in Remark 1.2 (SN1).

3. Results

3.1. Juxtacrine signalling and simplistic protrusions

For juxtacrine signalling on a hexagonal lattice, without protrusions, we set

$$\omega_J(\Delta j, \Delta k) = \begin{cases} \frac{1}{6} & \text{if } (\Delta j, \Delta k) \in S_1, \\ 0 & \text{otherwise,} \end{cases} \tag{26}$$

so that

$$\Omega_{\bar{q},\bar{p}} = \frac{1}{3}\left[\cos(2\pi\bar{q}) + \cos(2\pi\bar{p}) + \cos(2\pi(\bar{q}+\bar{p}))\right]. \tag{27}$$

Notice that $\Omega_{\bar{q},\bar{p}}$ takes discrete values within the interval $[-0.5, 1]$. The modes that minimise Eq. (27) are those for which N and M are multiples of 3, thus $(\bar{q}, \bar{p}) \in \{(1/3, 1/3), (2/3, 2/3)\}$ and a pattern with wavelength 3 along the main directions of the hexagonal lattice emerges, provided $AB < -2$. In general, and depending on the initial conditions, such patterns may yield 1, 2 or 3 different cell types, as discussed in more detail below.

Considering protrusions, we first look at the more straightforward case where only the first ring of 12 non-neighbouring cells, R_2, is reached by protrusions. Here, signalling is weighted laterally by Eq. (26) and on R_2 by

$$\omega_P(\Delta j, \Delta k) = \begin{cases} \frac{1}{12} & \text{if } (\Delta j, \Delta k) \in S_2, \\ 0 & \text{otherwise.} \end{cases} \tag{28}$$

Figs. 1(c)–1(f) show the observable patterns for different values of ϵ, with initial conditions near the homogeneous steady state, obtained by solving Eq. (23)–Eq. (24). Notice that the limit case $\epsilon = 1$ has the extreme feature of no juxtacrine signalling, hence the small clusters of Delta-expressing cells in Fig. 1(f). Even for small values of ϵ, sparse patterns are evident.

We may then weight each signalling contribution with a factor $\epsilon > 0$ and define the combined weighting function $\omega = (1-\epsilon)\omega_J + \epsilon\omega_P$. Using this leads to

$$\begin{aligned} \Omega_{\bar{q},\bar{p}} = {} & \frac{(1-\epsilon)}{3}\left[\cos(2\pi\bar{q}) + \cos(2\pi\bar{p}) + \cos(2\pi(\bar{q}+\bar{p}))\right] \\ & + \frac{\epsilon}{6}\Big[\cos(4\pi\bar{q}) + \cos(2\pi(\bar{p}-\bar{q})) + \cos(4\pi\bar{p}) \\ & \quad + \cos(2\pi(2\bar{q}+\bar{p})) + \cos(2\pi(\bar{q}+2\bar{p})) \\ & \quad + \cos(4\pi(\bar{q}+\bar{p}))\Big]. \end{aligned} \tag{29}$$

In this case, minimising $\Omega_{\bar{q},\bar{p}}$ is trickier and therefore we consider a numerical approach. For different values of the long-range signalling strength ϵ, Fig. 2(a) shows the change of $1/|\Omega_{\min}|$ for increasing values of ϵ. Notice that $\Omega_{\max} = 1$ for all ϵ. Equal juxtacrine-protrusion weighting occurs when $\epsilon = 2/3$ $(\Omega_{\min}(2/3) \simeq -0.24)$. For each ϵ, the number of modes varies, as seen in Fig. 2(b). Notice that $\Omega_{\bar{q},\bar{p}} = \Omega_{1-\bar{q},1-\bar{p}}$ and, in fact, $\Omega_{\bar{q},\bar{p}}$ is symmetric with respect to the planes $\bar{q} = \bar{p}$ and $\bar{q} = 1 - \bar{p}$ for all ϵ. An interesting observation is that at around $\epsilon = 0.4$ there are a total of 8 minimising modes, contrasting to the single pair of modes for $\epsilon < 0.4$ and the 6 distinct modes for $\epsilon > 0.4$ (Figs. 2(d)–2(f), Video S1). The bifurcation observed in Fig. 2(b) at $\epsilon = 0.4$ is predicted independently of the Hill functions, and can be mathematically shown by solving, for ϵ,

$$\Omega_{\frac{1}{3},\frac{1}{3}}(\epsilon) = \Omega_{\bar{q},\bar{p}}(\epsilon) \tag{30}$$

and a minimising pair $(\bar{q}, \bar{p}) \notin \{(1/3, 1/3), (2/3, 2/3)\}$ (see SN1 for details). Figs. 2(g)–2(i) show some of the simulations for corresponding values of ϵ.

As discussed before, the critical wave numbers maximise the real part of the temporal eigenvectors. Equivalently, Fig. 2(c) shows $\max_{\bar{q},\bar{p}} \mathrm{Re}(\lambda^{\pm}_{\bar{q},\bar{p}})$ as a function of the relative weight parameter ϵ, corresponding to the critical $AB = 1/(\max_{\epsilon} \Omega_{\min}) \simeq -5.207$. Here, $\max_{\bar{q},\bar{p}}(\mathrm{Re}(\lambda^{\pm}_{\bar{q},\bar{p}})) > 0$ for all ϵ, and thus patterns are expected to emerge with the maximising wavelength modes. As suggested by Eq. (21)–Eq. (24), we may go a step further and work out the specific parameter regions for which $|AB|$ yields pattern formation. The phase diagrams in Fig. 3 (Video S2) represent the regions in the $r_t - b$ plane such that $AB < 1/\Omega_{\min}(\epsilon)$, or more specifically,

$$n^{*1-h} d^{*1-k}((1 + bn^{*h})(a + d^{*k}))^2 < -abhk\Omega_{\min}(\epsilon) \tag{31}$$

for different values of $\Omega_{\min}$ and corresponding ϵ. The ϵ-Collier model is robust with respect to the pair (r_t, b), corresponding to the trans-interactions strength and ligand inhibition strength parameters, respectively. Increasing ϵ from zero initially reduces the size of the discrete

Supplementary Note 3: Simulation parameters

Table 1 shows the model parameters used in the simulations shown in the main text. In all simulations, $h = k = 6$, $\nu = 1$, and the initial conditions $n_i(0)$ and $d_i(0)$ have arbitrary values around the respective homogeneous steady state (n^*, d^*): $n_i(0) \sim N(n^*, 0.01)$ and $d_i(0) \sim N(d^*, 0.01)$.

Figures	p_ℓ	ϵ	$\log_{10} r_t$	$\log_{10} b$	(n^*, d^*)
1c-1f	2.1	$\{0, 0.2, 0.6, 1\}$	8	2	$(0.744, 0.055)$
2g-2i	2.1	$\{0.2, 0.4, 0.6\}$	8	2	$(0.744, 0.055)$
3	2.1	$\{0, 0.2, 0.4, 0.8, 1\}$	8	2	$(0.744, 0.055)$
4	2.1	$\{0.09, 0.78\}$	8	2	$(0.744, 0.055)$
5a-5c	4	$\{0.2, 0.4, 0.6\}$	8	2	$(0.744, 0.055)$
6a-6c	$\{2, 3, 4\}$	0.6	8	2	$(0.744, 0.055)$
7b-7e	2.1	0.6	8	2	$(0.744, 0.055)$
8	-	$\{0, 0.2, 0.4, 0.6, 0.8, 1\}$	-	-	-
9	-	$\{0, 0.2, 0.4, 0.6, 0.8, 1\}$	-	-	-
10 (row 1)	2.1	$\{0, 0.2, 0.4, 0.6, 0.8, 1\}$	1	2	$(0.420, 0.646)$
10 (row 2)	2.1	$\{0, 0.2, 0.4, 0.6, 0.8, 1\}$	2	1	$(0.671, 0.523)$
10 (row 3)	2.1	$\{0, 0.2, 0.4, 0.6, 0.8, 1\}$	5	1.3	$(0.781, 0.181)$

Table 1. Simulation parameters.

References

Aranson, I. S. and Kramer, L. The world of the complex Ginzburg–Landau equation. *Reviews of Modern Physics*, 74(1):99, 2002.

Binshtok, U. and Sprinzak, D. *Modeling the Notch response*. Springer, 2018.

Bozzini, B., Gambino, G., Lacitignola, D., Lupo, S., Sammartino, M., and Sgura, I. Weakly nonlinear analysis of Turing patterns in a morphochemical model for metal growth. *Computers & Mathematics with Applications*, 70(8):1948–1969, 2015.

Bracewell, R. N. and Bracewell, R. N. *The Fourier transform and its applications*, volume 31999. McGraw-Hill New York, 1986.

Collier, J. R., Monk, N. A., Maini, P. K., and Lewis, J. H. Pattern formation by lateral inhibition with feedback: a mathematical model of Delta-Notch intercellular signalling. *Journal of Theoretical Biology*, 183(4):429–446, 1996.

Doelman, A., Kaper, T. J., and Zegeling, P. A. Pattern formation in the one-dimensional Gray–Scott model. *Nonlinearity*, 10(2):523, 1997.

Hamada, H., Watanabe, M., Lau, H. E., Nishida, T., Hasegawa, T., Parichy, D. M., and Kondo, S. Involvement of Delta/Notch signaling in zebrafish adult pigment stripe patterning. *Development*, 141(2):318–324, 2014.

Kondo, S. How animals get their skin patterns: fish pigment pattern as a live Turing wave. *Systems Biology*, pages 37–46, 2009.

Lawrence, P. A. and Struhl, G. Morphogens, compartments, and pattern: lessons from Drosophila? *Cell*, 85(7):951–961, 1996.

Liu, S., Xia, S.-N., Yan, R., Wan, Z.-H., and Sun, D.-J. Linear and weakly nonlinear analysis of Rayleigh–Bénard convection of perfect gas with non-Oberbeck–Boussinesq effects. *Journal of Fluid Mechanics*, 845:141–169, 2018.

McGough, J. S. and Riley, K. Pattern formation in the Gray–Scott model. *Nonlinear Analysis: Real World Applications*, 5(1):105–121, 2004.

Meinhardt, H. Models of biological pattern formation: common mechanism in plant and animal development. *International Journal of Developmental Biology*, 40(1):123–134, 2003.

Meinhardt, H. Models of biological pattern formation: from elementary steps to the organization of embryonic axes. *Current Topics in Developmental Biology*, 81:1–63, 2008.

O'Dea, R. D. and King, J. R. Multiscale analysis of pattern formation via intercellular signalling. *Mathematical biosciences*, 231(2):172–185, 2011.

Stephenson, L. E. and Wollkind, D. J. Weakly nonlinear stability analyses of one-dimensional Turing pattern formation in activator-inhibitor/immobilizer model systems. *Journal of Mathematical Biology*, 33(8):771–815, 1995.

Stuart, J. On the non-linear mechanics of wave disturbances in stable and unstable parallel flows part 1. the basic behaviour in plane Poiseuille flow. *Journal of Fluid Mechanics*, 9(3):353–370, 1960.

Tabata, T. and Takei, Y. *Morphogens, their identification and regulation*. Oxford University Press for The Company of Biologists Limited, 2004.

Turing, A. The chemical basis of morphogenesis. *Philosophical Transactions of the Royal Society of London. Series B, Biological Sciences*, 237(641):37–72, 1952.

Vincent, J.-P. and Briscoe, J. Morphogens. *Current Biology*, 11(21):R851–R854, 2001.

Watson, J. On the non-linear mechanics of wave disturbances in stable and unstable parallel flows Part 2. The development of a solution for plane Poiseuille flow and for plane Couette flow. *Journal of Fluid Mechanics*, 9(3):371–389, 1960.

Wollkind, D. J. and Segel, L. A. A nonlinear stability analysis of the freezing of a dilute binary alloy. *Philosophical Transactions of the Royal Society of London. Series A, Mathematical and Physical Sciences*, 268(1191):351–380, 1970.

Wollkind, D. J. and Vislocky, M. An interfacial model equation for the bifurcation of solidification patterns during lpee processes. *Earth-Science Reviews*, 29(1-4):349–368, 1990.

Wollkind, D., Oulton, D., and Sriranganathan, R. A nonlinear stability analysis of a model equation for alloy solidification. *Journal de Physique*, 45(3):505–516, 1984.

Wollkind, D. J., Manoranjan, V. S., and Zhang, L. Weakly nonlinear stability analyses of prototype reaction-diffusion model equations. *Siam Review*, 36(2):176–214, 1994.